ChemComm

Accepted Manuscript

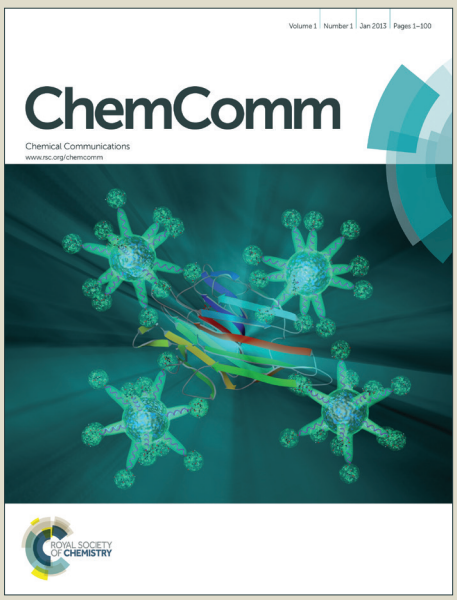

ROYAL SOCIETY OF CHEMISTRY

www.rsc.org/chemcomm

ChemComm

COMMUNICATION

Super-paramagnetic nano-Fe_3O_4/Graphene for visible-light-driven Hydrogen Evolution

Received 00th January 20xx,
Accepted 00th January 20xx

DOI: 10.1039/x0xx00000x

www.rsc.org/

Wenyan Zhang [a,b,c], *Chao Kong*[a,b] and *Gongxuan Lu*[a*]

A super-paramagnetic nano-architecture, which could be separated and re-dispersed easily for reusing, was designed for effective dye-sensitized H_2 evolution. By the enhancement of electron-transfer and surface-repair ability of graphene, the visible-light-driven hydrogen evolution rate over exposed Pt (111) facet loaded Fe_3O_4/GO catalyst was remarkably enhanced.

In the past decades, over-consumption of fossil fuel and related environmental pollution problems makes scientists urgent to search for efficient, clean and renewable energy resource to solve those energy crisis[1]. Hydrogen is recognized to be an ideal next-generation energy because of its higher combustion enthalpy than conventional fuels and "zero-pollution" (yielding only water after oxidation)[2]. Splitting water by solar energy is a promising strategy for hydrogen generation[3]. Plenty of advances have been reported to enhance the efficiency of visible-light-driven H_2 evolution, including the application of high active catalysts, improving the charge separation by the aids of carbon materials, expanding the photo-responsive range by dye sensitization and modify the dispersion of catalyst in reactive system to improve the reactive interface area between the catalyst and the solution[4-6].

Some problems still exist in the H_2 evolution reaction (HER) research field. For one thing, the H_2 evolution activity and stability are far from satisfactory[1-3,7]. For another, it is expensive and time-consuming to separate the photo-catalysts and co-catalysts from the reactive system[1-3,7,8]. High cost of catalysts has become one of the bottlenecks for the commercial development of visible-light-driven hydrogen evolution. It is highly desirable to develop the appropriate catalyst which not only have satisfactory activity and stability, but could be conveniently separated from and re-dispersed into the reactive solution for recycling use to decreasing the catalytic costs. Furthermore, the danger of hydrogen explosion could not be ignored especially for the large scale production and transportation of hydrogen[9]. Separating the photo-catalysts from reactive system in time is an effective way to slow down the loss of catalyst, as a result improving the effectiveness of catalysts of large scale H_2 evolution.

During the past decades, a variety of strategies have been employed to improve the photocatalytic performance of photo-catalysts[10,11]. In particular, the graphene has been applied to build graphene-based photo-catalysts[12,13]. Due to its high conductivity, superior electron mobility and extremely specific surface area, the graphene could effectively enhance the photocurrent density and hydrogen generation rate[14].

Magnetic nano-materials have also received much attention at present. Because of their sensitive response to external magnetic field, functionalized magnetic nano-materials have shown wide application for the drug delivery, dual imaging, recoverable catalyst, bio-sensors, and selective recovery of metal ions or molecules[15, 16]. Although there has been extensive research on the photo-catalytic degradation of organic dye by magnetic, little attention has been paid to their application in the HER field. In fact, magnetic separation of catalyst could endow the HER process with a "magnetic switch". It is convenient to realize control the reaction process by regulating the magnetic field outside the HER system. That could inevitably enhance the safety of HER reactive system.

Herein, we report, for the first time, a super-paramagnetic nano-architecture for the dye-sensitized H_2 evolution under visible light irradiation ($\lambda \geq 420$ nm) over exposed Pt (111) facet loaded Fe_3O_4 catalyst. As illustrated by Scheme 1, the nano-architecture is composed of ternary components: (1) The Fe_3O_4 hollow spheres to provide the catalyst with super-paramagnetic property and sufficient hydrophilic groups; (2) The graphene (GR) sheets enhance transfer the photo-generated charge and modify the surface of Fe_3O_4; (3) Active Pt quantum dots that distribute uniformly across the GR sheets to act as the co-catalyst. Such nano-architecture material exhibits favourable activity and stability for visible light driven H_2 evolution. Besides, the composite catalyst responds sensitively to external magnetic field. It is convenient to separate the catalyst from reactive system and re-disperse them into the solution for recycling use.

Photo-catalysts were synthesized by hydrothermal method (details in ESI†). In Fig. 1 (a), the diffraction peaks could be assigned to different crystal planes of cubic Fe_3O_4 (JCPDS#65-3107). Diffraction peaks of Pt and GR were not obvious in the XRD pattern though the X-ray photoelectron spectroscopy (XPS) in Fig. 2 (a)

[a] *State Key Laboratory for Oxo Synthesis and Selective Oxidation, Lanzhou Institute of Chemical Physics, Chinese Academy of Science, Lanzhou 730000, China*
[b] *University of Chinese Academy of Science, Beijing 10080, China.*
[c] *College of Material Engineering, Jinling Institute of technology, Nanjing, China*
Electronic Supplementary Information (ESI) available: [details of any supplementary information available should be included here]. See DOI: 10.1039/x0xx00000x

demonstrated that the Fe_3O_4@Pt and Fe_3O_4@Pt@GR catalysts are composed of Fe, C, O and Pt elements (Fig.1e). Furthermore, the XPS peaks at 70.9 eV and 74.3 eV could be assigned to the Pt $4f_{7/2}$ and Pt $4f_{5/2}$ states, respectively. The Pt 4f XPS spectra indicate that the Pt element exists as metallic state in the Fe_3O_4@Pt and Fe_3O_4@Pt@ GR [17].

Fig.1 (b) reveals that the Fe_3O_4 are hollow spheres which were assembled by lots of Fe_3O_4 nano-crystals. The 0.29 and 0.25 nm interlayer distance could be assigned to the (220) and (311) planes of cubic Fe_3O_4, respectively. As to the Fe_3O_4@Pt, some gray quantum dots co-exist with the Fe_3O_4 nano-crystals (Fig.1 (c)). The gray quantum dots shows 0.19 and 0.23 nm inter-planar distances, which could respectively be assigned to the (100) and (111) plane of tetragonal Pt. For the Fe_3O_4@Pt@ GR, the Fe_3O_4 microspheres are anchored on the GR sheets to form a two-dimensional nano-architecture (Fig.1 (d)). Moreover, there are large amounts of gray quantum dots connected on the GR surface. The quantum dots on GR have the interlayer distances of 0.19 and 0.23 nm, which also respectively corresponds to the (100) and (111) planes of Pt. The result indicates that the GR offered a good template for the growth of Pt quantum dots.

It is interesting to find that the the Pt dots tends to expose their (100) planes in the Fe_3O_4@Pt catalyst while the dots mainly expose their (111) facets in the Fe_3O_4@Pt@ GR, as shown in Fig. 1 (g). It seems that the GR sheets may have inductive effect on the preferential growth of Pt. Similar phenomenon has also been reported for the synthesis of single crystal Pt nano-sheets in molten salt medium system[18].

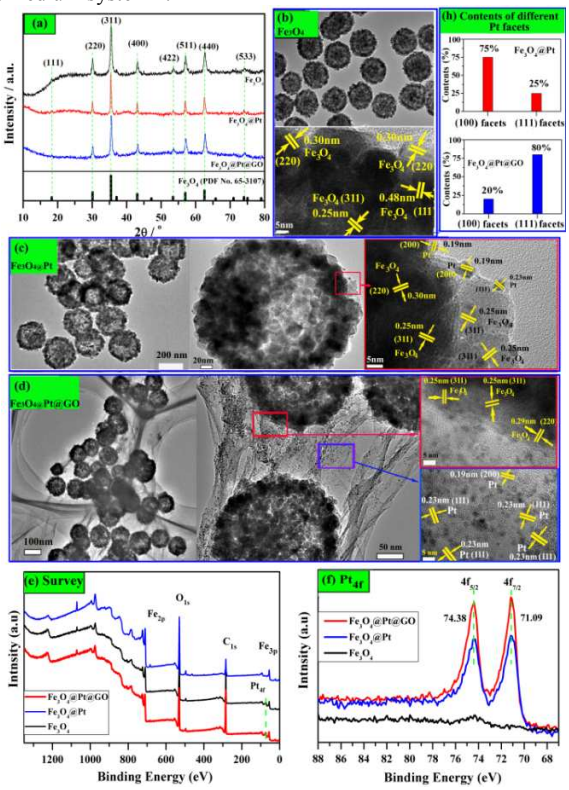

Fig.1 (a) X-ray diffraction (XRD) patterns of Fe_3O_4, Fe_3O_4@Pt, Fe_3O_4@Pt@GR; TEM image and HRTEM image for (b) Fe_3O_4, (c) Fe_3O_4@Pt and (d) Fe_3O_4@Pt@GR; (e) Survey and (f) Pt 4f scan spectra of Fe_3O_4@Pt and Fe_3O_4@Pt@ GR; (g) different contents of exposed Pt facets for Fe_3O_4@Pt and Fe_3O_4@Pt@GR

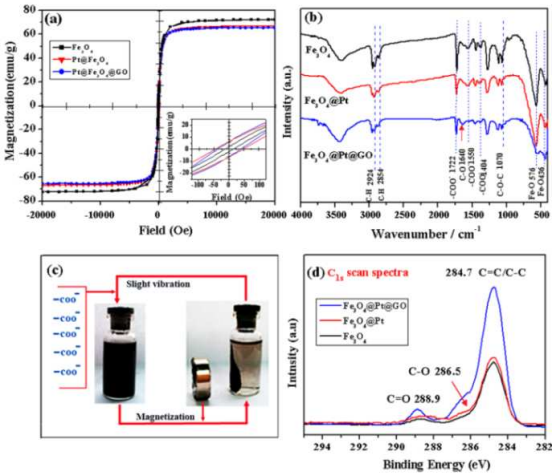

Fig. 2 (a) Magnetic hysteresis curves of Fe_3O_4, Pt@Fe_3O_4 and Pt@Fe_3O_4@GR at room temperature (b) FTIR spectra of Fe_3O_4, Pt@Fe_3O_4 and Pt@Fe_3O_4@GR (c) XPS survey spectra of Fe_3O_4, Pt@Fe_3O_4 and Pt@Fe_3O_4@GR. (d) C_{1s} scan spectra of Fe_3O_4@Pt and Fe_3O_4@Pt@GR.

As shown in Fig. 2 (a), the Fe_3O_4 spheres show very little remnant magnetization and coercivity, indicating that the spheres are super-paramagnetic iron oxide. The super-paramagnetic property of Fe_3O_4 spheres is consistent with their XRD and HRTEM characterizations that the spheres are composed of smaller nano-crystals[19]. The super-paramagnetic property of Fe_3O_4 could be remained when we assembled it with Pt and GR to form the nano-architecture of Pt@Fe_3O_4, and Pt@Fe_3O_4@GR. The saturation magnetization (*Ms*) of Pt@Fe_3O_4 and Pt@Fe_3O_4@ GR could reach 63 and 61 emu/g, respectively. The *Ms* is large enough for the catalyst to be magnetized and separated easily from the solution for recycle use by utilizing magnet field (Fig. 3(b)). The catalysts could also be demagnetized only by removing the external magnet field due to its super-paramagnetic nature. The catalysts could disperse well in water dispersion to form an aqueous solution (Fig. 3 (c)). This is related to the carboxyl groups (COO^-) connected on the catalysts (Fig. 3 (b)). The COO^- groups could not only improve the hydrophilicity of catalysts but enhance their water-dispersion via electrostatic repulsive force[20]. The nano-architecture could therefore be re-dispersed in water again by slight shaking, as shown in Fig. 3 (b). Furthermore, the intensity of Fe-O groups decreased obviously with the addition of GR, indicating that the GR may "cover" or interact with the Fe-O groups on the surface of Fe_3O_4 microspheres. In agreement with the FTIR results, the peaks at 284.7, 286.5, and 288.9 eV also verify the existence of C=C, C-O and C=O bonds (Fig. 3 (d))[21]. Intensity of the C-O and C=O groups is much lower than that of the C=C groups, indicating that most of the oxygen-containing groups on raw GO sheets were reduced during the hydrothermal process.

The H_2 evolution test has been carried out to compare the activity and stability of different catalysts, as shown in Fig. 3 (a). In the first run, small amounts of H_2 (25 μmol) were produced in Eosin Y (EY)-Fe_3O_4 system after 6 h irradiation ($\lambda \geqslant 420$ nm). H_2 evolution was enhanced to 432 μmol in 6 h when the Pt@Fe_3O_4 was used as

catalyst. The enhancement of H_2 evolution could be attributed to the high activity and low over-potential of Pt for proton reduction[22]. 614 μmol H_2 was produced over the EY-sensitized Pt@Fe_3O_4@GR photo-catalyst in 6 h, which were 24.6 and 1.4 times higher than that of Fe_3O_4 and Pt@Fe_3O_4. Moreover, Pt@Fe_3O_4@GR exhibits better stability than the Fe_3O_4 and Pt@Fe_3O_4. In the 2nd run, the H_2 production over Pt@ Fe_3O_4@GR could be revived to 95.8% while that over the Pt@Fe_3O_4 was only recovered to 78%. Therefore, the stability of catalyst could be improved obviously by decorating the products with GR sheets.

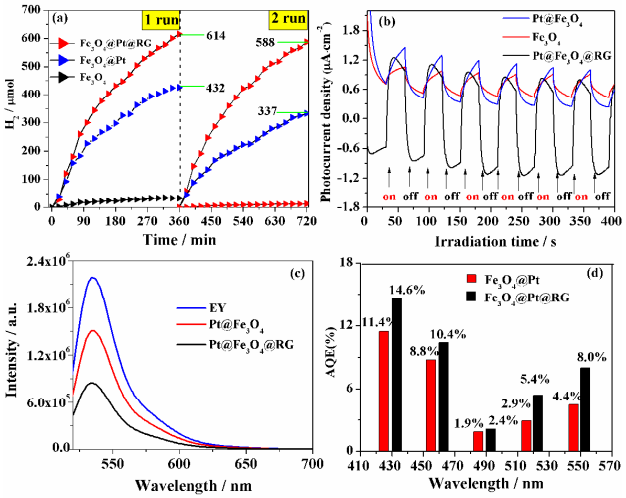

Fig. 3 (a) H_2 evolution from EY photosensitized systems (1.0×10^{-3}mol/L) in 100 mL of 10% (v/v) TEOA aqueous solution (pH=11, λ≥420 nm). (b) Photo-current curves in 0.1 mol/L Na_2SO_4 solutions Fe_3O_4. (c) Photo-luminescence of EY, EY-Fe_3O_4@Pt and EY-Fe_3O_4@Pt@GR (d) Apparent quantum efficiencies (AQEs) of H_2 evolution under the irradiation at different wavelengths.

Table 1 Decay parameters of EY in the presence of Fe_3O_4@Pt and Fe_3O_4@Pt@GR.

System	Lifetime (ns)	Pre-exponential factors A	A	χ^2
EY	τ=1.21	0.0736	0.33	1.00
Fe_3O_4@Pt	τ1=0.806	A1=0.0416	0.38	1.00
	τ2=1.41	A2=0.0385		
Fe_3O_4@	τ1=1.01	A1=0.067	0.64	1.00
Pt@GR	τ2=1.67	A2=0.0125		

The concentrations of dyes and catalysts were 1×10^{-6} mol/L and 10 mg/mL, respectively. Single-exponential fit for EY. Double-exponential fit for EY-Fe_3O_4@ Pt and EY-Fe_3O_4@Pt@GR.

The effect of GR is further investigated by the photo-current and photo-luminescence test. As shown in Fig. 3 (b), the EY-Fe_3O_4@Pt@ GR exhibits higher photocurrent than the EY-Fe_3O_4 and EY-Fe_3O_4@Pt. As a zero-band semiconductor, the GR sheets could transfer the photo-generated electron effectively to the Pt active sites. The large enhancement of photo-current indicates excellent conductive effect of GR sheets. Besides, the luminescent intensity of EY decreased dramatically with the addition of Fe_3O_4@Pt@GR (Fig. 3 (c)), which also implies effective electron transfer between the excited EY* and the catalysts. Fluorescence lifetime of EY was investigated to reveal more information about the energy transfer process (Table 1). The emission of EY exhibits a single-exponential decay and its lifetime is 1.21 ns. The single-exponential decay divided into a short and a long exponential decay when the Fe_3O_4@Pt or Fe_3O_4@Pt@GR catalyst was tested (Table 1). The long and short emission decay could respectively be assigned to the unbounded EY and the EY linked to the catalyst[23]. It is apparent that the EY-Pt@Fe_3O_4@GR exhibits longer fluorescence lifetime than the EY-Fe_3O_4@Pt system, indicating that the GR could prolong the lifetime of excited EY in the TEOA solution[24]. Longer lifetime could leave more time for the photo-electrons to pass through the GR sheets before being quenched by the sacrifice reagent TEOA, as a result improving the H_2 evolution.

The effect of GR on the e^--h^+ separation may not be the only reason for the enhancement of H_2 evolution. The surface states could also affect the efficiency of H_2 evolution. In **Fig. S1(a-d)**, the $Fe_{2p1/2}$ and $Fe_{2p3/2}$ peaks can be de-convoluted by six peaks around 710, 712, 718, 723, 725 and 732 eV. The two satellite peaks around 718 and 732 eV could be assigned to Fe^{3+} in the Fe_2O_3 phase, indicating that the surface of microspheres are slightly oxidized in the air environment[25]. The other four peaks respectively correspond to the Fe^{2+} (710, 723 eV) and Fe^{3+} (712, 725 eV) in the Fe_3O_4 phase. Area ratio of the Fe^{3+}/Fe^{2+} in Fe_3O_4 phase were calculated to be 1.27/1, 0.90/1 and 1.20/1 for the Fe_3O_4, Fe_3O_4@Pt, and Fe_3O_4@Pt@GR (Fig. S1(d))[20]. The Fe^{3+}/Fe^{2+} ratio on Fe_3O_4@Pt surface deviates seriously from that on the surface of Fe_3O_4. The result indicates lots of surface defects existing on the surface of Fe_3O_4@Pt. As for the Fe_3O_4@Pt@GR, the Fe^{3+}/Fe^{2+} ratio on its surface revives back to 1.20/1. The decreasing of Fe^{3+}/Fe^{2+} ratio indicates that the GR could "repair" or "cover" the surface defects of Fe_3O_4 microspheres[26]. As a result, application efficiency of the photo-generated charges could be improved because more photo-electrons were separated and transferred to the co-catalysts before quenched by the surface defects. In order to investigate the effect of Fe_3O_4 on the performance of hydrogen evolution, the hydrogen evolution rate over Pt@GR was also collected and compared with that of Fe_3O_4@Pt@GR (Fig. S11). H_2 evolution over the Fe_3O_4@ Pt @GR was lower than that over the Pt@GR, indicating that some photo-electrons were quenched by the defects on the Fe_3O_4 surface.

The O 1s spectra are also investigated to reveal more information of the surface. The O 1s spectra of photo-catalysts could be de-convoluted into three peaks around 530, 531 and 533 eV, which respectively corresponds to the oxygen in the Fe_3O_4 crystal lattice oxide oxygen (O^{2-}), hydroxyl (–OH), and absorbed water (H_2O)[27]. Relative content of different oxygen species are summarized in **Fig. S1(h)**. The amount of O^{2-} on the Fe_3O_4@Pt surface is obviously less than that on the surface of Fe_3O_4. The decreasing of O^{2-} indicates plenty of low oxygen coordination defects existing on the Fe_3O_4@Pt surface. Those surface defects provide more "annihilations" sites for the photo-generated electrons, and therefore aggravate the failing of photo-current and H_2 evolution. Surface defects may also decrease the stability of catalysts due to the surface corrosion on in the alkaline TEOA reactive solution (pH=11).

Furthermore, different exposed facet of Pt quantum dots may also have effect on the H_2 evolution (Fig. 1 (g)). The Pt (111) facets have three advantages over its (100) facet for the production of H_2[28, 29]. Firstly, the Fermi energy of Pt (111) and (100) facet is respectively about -1.29 eV and -1.95 eV, suggesting that the photo-electrons are more feasible to be transferred to the (111) facets[28-31]. Secondly, the

number of chemisorbed H atoms on the Pt (111) facets was much more than that on the Pt (100) facets. Besides, the Pt (111) facets have more suitable sites for the recombination H-H atoms. These advantages result in the higher activity of Pt (111) facets for the H_2 evolution. As a result, the better performance of Fe_3O_4@Pt@GR is also relevant to the large amounts of Pt (111) facets on the GO sheets.

Apparent quantum efficiencies (AQEs) of the EY-Fe_3O_4@Pt and EY-Fe_3O_4@Pt@GR system had also been collected from 430 to 550 nm (Fig. 3 (d)).The EY-Fe_3O_4@Pt@GR system show higher AQE than the EY-Fe_3O_4@Pt system under each irradiation wavelength. The improvement of AQE could also be related to the conductive and "repair" effects of GR, as well as the advantages of Pt (111) face. According to above results, a mechanism could be proposed for the H_2 evolution, as shown in Scheme 1. When the Fe_3O_4@Pt@GR is introduced into the EY-TEOA solution system, the EY molecules could adsorb on the surface of GR sheets, the Fe_3O_4 micro-spheres, and the Pt (111) facets by physical or chemistry adhesion. Upon visible light irradiation, the electrons at the highest-occupied molecular orbital (HOMO) of EY could absorb the light energy and be excited to the lowest-unoccupied molecular orbital (LUMO). Inevitably, some photo-electrons may be quenched by defects on the Fe_3O_4 surface. Most of the photo-generated electrons are trapped by the GR sheets due to its excellent electron-accepting and electron-transporting ability.The trapped electrons then pass through the GR sheets, accumulated on the Pt (111) facet and lead to the hydrogen production from water.

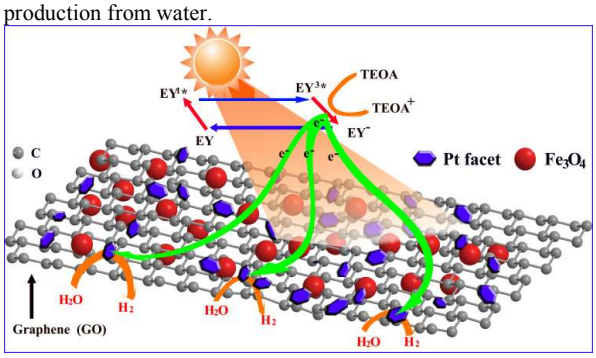

Scheme1 Proposed photocatalytic mechanism for hydrogen evolution over Fe_3O_4@Pt@GR photocatalyst under visible light irradiation

In summary, magnetic nano-architecture was synthesized by hydrothermal method for dye-sensitised hydrogen evolution. The super-paramagnetic Fe_3O_4@Pt@GR catalyst shows sensitive response to outside magnetic field. It is convenient to separate the catalyst from reactive system and re-disperse them into dye-sensitized reactive system for reuse. GR play a crucial role in improving the activity and stability of the magnetic photo-catalyst. This report may offer a feasible strategy to improve the efficiency and stability of magnetic catalysts, as well as reduce the cost for visible-light-driven H_2 evolution.

This work is supported by the NSF of China (grant no. 21433007, 21173242) and the 973 and 863 Programs of Department of Sciences and Technology of China (2012AA051501, 2009CB220003) respectively.

Notes and references

[a]*State Key Laboratory for Oxo Synthesis and Selective Oxidation, Lanzhou Institute of Chemical Physics, Chinese Academy of Science, Lanzhou 730000, China*
[b]*University of Chinese Academy of Science, Beijing 10080, China.*
[c]*College of Material Engineering, Jinling Institute of technology, Nanjing, China*
[*]*Corresponding author: E-mail: gxlu@lzb.ac.cn.*
Tel.: +86-931-4968 178. Fax: +86-931-4968 178.

†Electronic Supplementary Information (ESI) available: [details of any supplementary information available should be included here]. See DOI:

1 Kazuhiko Maeda, J.Photochemistry and Photobiology C: Photochemistry Reviews, 2011, **12**, 237
2 Z. Han, R. Eisenberg, Acc. Chem. Res. 2014, **47**, 2537
3 A. Clough, J. Yoo, M. Mecklenburg, S. Marinescu, J. Am. Chem. Soc. 2015, **137**, 118 -121
4 S. Min, G. Lu, J. Phys. Chem. C. 2012, **116**, 19644
5 C. Kong, S. Min, G. Lu. ACS Catal 2014, **4**, 2763
6 W.i Zhang, J. Hong, J. Zheng, Z. Huang, J. Zhou, R. Xu, J. Am. Chem. Soc. 2011, **133**, 20680
7 C. Kong, S, Min, G, Lu, Chem. Commun., 2014, **50**, 5037
8 H. Yan, J. Yang, G. Ma, G. Wu, X. Zong, Z. Lei, J. Shi and C. Li, J. Catal., 2009, **266**, 165
9 B. Angers, A. Hourri, P. Benard, E. Demael, S. Ruban, S. Jallais, Int J Hydrogen Energy, 2014, **39**, 6210
10 Q. Xiang, J. Yu, J. Phys. Chem. Lett., 2013, **4**, 753−759
11 Q. Xiang, J. Yu, M. Jaroniec, Chem. Soc. Rev. 2012, **41**, 782–796.
12 X. Li, J. Yu, J. Low, Y. Fang, J. Xiao, X. Chen, J. Mater. Chem. A, 2015, **3**, 2485-2534.
13 S. Liang, J. Zhu, C. Wang, S. Yu, H. Bi, X, Liu, X. Wang, Appl. Surf. Sci., 2014, **292**, 278-284
14 P. Dubey, P. Tripathi, R. Tiwari, A. Sinha, O. Srivastava, Int. J. Hydrogen Energy, 2014, **39**, 16282-16292
15 J. Gao, X. Ran , Chu nmeng. Shi, H. Cheng, T. Cheng, Y. Su, Nanoscale, 2013, **5**, 7026
16 Dupont, J. Luyten, M. Bloemen, T. Verbiest, K. Binnemans, Ind. Eng. Chem. Res. 2014, **53**, 15222
17 F. Li, Y. Guo, Y. Liu, J. Yan, W. Wang, J. Gao. Carbon, 2014, **67**, 617.
18 13 S. Yang, P. Qiu, G. Yang, Carbon, 2014, **77**, 1123.
19 S. Xuan, Y. Wang, J. Yu, K. Leung, Chem. Mater., 2009, **21**, 5079
20 J. Ge, Y. Yin, J. Mater. Chem., 2008, **18**, 5041
21 F. Chen, F. Yan, Q. Chen, Y. Wang, L. Han, Z. Chen, S. Fang, Dalton Trans., 2014, **43**, 13537
22 C. Kong, S. Min, G. Lu. Chem. Commun. 2014, **50**, 9281
23 S. Min, G. Lu, J. Phys. Chem. C. 2011, **115**, 13938
24 Z. Xiong, L. Zhang, J. Ma, X. Zhao, Chem. Commun. 2010, **46**, 6099
25 G. Bhargava，I. Gouzman, C. Chun, T. Ramanarayanan, S. Bernasek, Appl. Surf. Sci. 2007, **253**, 4322
26 J. Zhu, G. Zhang, X. Yu, Q. Li, B. Lu, Z. Xu, Nano Energy 2014, **3**, 80
27 X. Hu, M. Ma, M. Zeng, Y. Sun, L. Chen, Y. Xue, Tao Zhang, X. Ai, R. Mendes, M. Rümmeli, L. Fu, Appl. Mater. Interfaces 2014, **6**, 22527
28 R. Narayanan, M. El-Sayed, Nano Letters, 2004, **4**, 1343
29 E. Cui, G. Lu, J. Phys. Chem. C. 2013, **117**, 26415
30 Z. Li, G. Lu, J. Mol. Catal.(China), 2014. **28**, 351
31 B. Li, G. Lu, J. Mol. Catal.(China), 2013, **27**, 181.

